



## EFFECTS OF POLYDISPERSITY OF AGGREGATES AND PRIMARY PARTICLES ON RADIATIVE PROPERTIES OF SIMULATED SOOT

T. L. FARIAS,<sup>a</sup> Ü. Ö. KÖYLÜ,<sup>b†</sup> and M. G. CARVALHO<sup>a</sup>

<sup>a</sup>Mechanical Engineering Department, Instituto Superior Técnico, 1096 Lisbon, Portugal and

<sup>b</sup>Chemical Engineering Department, Yale University, New Haven, CT 06520, U.S.A.

(Received 24 April 1995)

**Abstract**—The effects of primary particle (particle) and cluster (aggregate) size distributions on absorption and scattering properties of simulated soot were studied both computationally and theoretically. Computational methods involved the solution of the volume integral equation formulation of Maxwell's equations using the method of moments, based on the ICP algorithm. The theoretical methods employed Rayleigh–Debye–Gans approximation for mass fractal-like aggregates (RDG-FA) formed by small particles. An extension of the RDG-FA formulation was proposed to account for polydisperse particle sizes, based on a volume correction approach. Differential and total scattering as well as absorption cross sections were considered for morphologies representative of soot found in flame environments. Aggregates were constructed using a sequential algorithm which mimics mass fractal-like structures. Log-normal and normal (Gaussian) probability density functions were employed to consider polydisperse populations of aggregates and particles, respectively. Over the range of evaluation, the effects of aggregate and particle polydispersity were negligible for the angular scattering pattern in the power-law regime. Furthermore, absorption cross section was similarly affected by polydispersity of aggregates and particles. Finally, the RDG-FA predictions generally agreed with the ICP results within 10%, confirming its applicability to predict mean optical properties of polydisperse populations of soot aggregates and particles.

### INTRODUCTION

Most practical flames contain soot, which increases heat transfer rates significantly due to continuum radiation. Knowledge of radiative properties of soot, in particular, emissivity, is necessary in order to predict radiation heat transfer from soot containing flames.<sup>1</sup> Thus, an accurate understanding of the absorption and scattering properties of soot is essential in a variety of practical applications, such as natural fires, industrial boilers and internal combustors. Additionally, soot optical cross sections are also needed to interpret *in situ* light scattering and extinction measurements for predicting soot concentration and morphology.<sup>2</sup>

Generally, soot consists of primary particles (particles) that individually satisfy the small particle (Rayleigh) scattering theory. Nevertheless, in their early stages of formation, these particles combine into branched clusters (aggregates) which may contain up to several hundreds of particles. Therefore, soot radiative properties cannot be treated reasonably by simple spherical models such as Mie theory, see Köylü and Faeth,<sup>2,3</sup> and references cited therein. In spite of these morphological complexities, however, recent developments in fractals permitted soot to be characterized as mass fractal-like aggregates.<sup>4,5</sup> This, in turn, made it possible to represent different size and shape soot aggregates with a fractal dimension, which seemed to be an invariable property in flames, fortunately, due to cluster-cluster aggregation mechanism.<sup>6–8</sup>

Jones<sup>9</sup> was among the first ones to develop a method for the scattering and absorption cross sections of soot, considering cluster structures formed by small particles, based on the derivation originated from Saxon's<sup>10</sup> integral equation formulation. Berry and Percival<sup>11</sup> expanded this

†To whom all correspondence should be addressed.

formulation by employing fractal ideas. Their work indicated that multiple scattering from aggregates with fractal dimensions less than two was negligible, as long as the particles constructing aggregates were in the Rayleigh regime. This has led to the application of approximate Rayleigh–Debye–Gans theory for fractal aggregates (RDG-FA), such as soot, see Köylü and Faeth,<sup>2</sup> Julien and Botet,<sup>4</sup> Dobbins and Megaridis,<sup>5</sup> Martin and Hurd,<sup>12</sup> Mountain and Mulholland,<sup>13</sup> and references cited therein. The approximate RDG-FA theory is of great interest since it directly relates aggregate morphology to optical cross sections, making practical applications tractable. Consequently, several experimental<sup>3,8,14</sup> and computational<sup>15–17</sup> evaluations of RDG-FA theory have been undertaken in order to identify its limitations to treat soot optical properties. Experimental evaluations of Köylü and Faeth<sup>3,8</sup> included angular light scattering and extinction measurements, which yielded encouraging performance of the RDG-FA approximation within experimental uncertainties of finding higher moments of the polydisperse aggregate populations and soot refractive indices. Because of these difficulties, Farias et al<sup>17</sup> studied optical cross sections of monodisperse soot aggregates based on the solution of the volume integral equation formulation, using the ICP algorithm of Iskander et al.<sup>18</sup> The ICP method provided a more exact treatment of aggregate scattering since it includes multiple scattering and self-induced terms. The results of Farias et al<sup>17</sup> indicated that RDG-FA approximate theory agreed with ICP predictions within computational uncertainties (ca. 10%) for morphologies typical of soot aggregates. Similar results were reached independently by Singham and Bohren,<sup>15</sup> and Mulholland et al.<sup>16</sup> All these investigations, however, were limited to monodisperse aggregate populations to avoid complications of the polydisperse aggregates. Additionally, both ICP and RDG-FA predictions were based on the assumption that the particle diameters within an aggregate were constant, i.e. monodisperse.

Unfortunately, the studies of soot morphology revealed that the aggregate as well as primary particle sizes had some distributions in flame environments, because of complex nucleation and aggregation processes involved.<sup>6–8,19</sup> Specifically, the number of particles in aggregates appeared to satisfy log–normal distribution functions, while particle diameters were approximately represented by normal (Gaussian) distributions.<sup>7</sup> These experimental observations suggest that aggregate and particle size distributions should be taken into account to correctly model soot radiative properties in flames. Although, the polydispersity of aggregates have previously received some attention experimentally,<sup>3,8</sup> a definitive assessment of its effects on the optical properties were very limited due to experimental uncertainties of knowing aggregate size distributions. Additionally, the particles have usually been considered monodisperse<sup>3,8,17,25</sup> since the standard deviations of particle size distributions were 15–25% of the mean values, small compared to the broad range of aggregate size distributions. However, even a narrow distribution of particles may still influence optical characteristics of aggregates considerably. This is quite obvious for unaggregated small particles, for which the scattering and absorption are proportional to sixth and third powers of particle diameter, respectively. Correspondingly, the effect of particle polydispersity could be significant since the optical cross sections of aggregates are expressed in terms of particle properties. Thus, the main objective of the present study was to investigate the effects of polydispersity of aggregates and particles on soot optical properties. Differential scattering, total scattering and absorption cross sections were computed using both ICP method and RDG-FA formulation for typical soot-like morphologies. An extension of the RDG-FA approximation was proposed to account for polydisperse populations of particle sizes, based on a volume correction approach.

## THEORETICAL METHODS

### *ICP solution*

More exact solution methods for calculating optical cross sections of soot aggregates consisting of assemblies of small particles were reviewed and compared by Ku and Shim,<sup>20</sup> considering the formulations of Purcell and Pennypacker,<sup>21</sup> Jones,<sup>9</sup> and Iskander et al.<sup>18</sup> The solution by Goedecke and O'Brien<sup>22</sup> was not included in their work since it was almost identical to the ICP approach of Iskander et al.<sup>18</sup> Although different in their mathematical approaches, all these methods involve the solution of an identical system of linear equations with slightly different coefficients. In terms

of level of accuracy and soundness of the derivation, Ku and Shim<sup>20</sup> concluded that the ICP formulation was superior to the rest since it includes multiple scattering terms up to third order and a self-interaction term. The performance of ICP was also compared to the exact solution yielding differences that never exceeded 2–3% for morphologies typical of soot.<sup>23</sup> Therefore, the ICP formulation was adopted in the present investigation due to computational time and storage considerations. The main results of ICP approach will be briefly discussed in the following, since the details can be found in Iskander et al,<sup>18</sup> and Ku and Shim.<sup>20</sup>

The ICP formulation treats aggregates by dividing them into small computational cells, which individually act as dipoles (Rayleigh limit). Then, the solution of the scattering of an electromagnetic wave by an aggregate of  $N$  spherical particles of diameter  $d_p$  starts by obtaining the internal field of each primary particle,  $\mathbf{E}_j$ , from a system of  $3N \times 3N$  linear equations of the form:

$$\mathbf{E}_j = \left( \frac{3}{m^2 + 2} \right) \mathbf{E}_{inc,j} + \left( \frac{i}{3} \right) \left( \frac{m^2 - 1}{m^2 + 2} \right) \sum_{k=1, \neq j}^N x_{p_k}^3 \mathbf{T}_{jk} \mathbf{E}_k + s_j \mathbf{E}_j; \quad j = 1, 2, \dots, N, \quad (1)$$

where  $m = n + i\kappa$  is the complex refractive index ( $i = \sqrt{-1}$ ),  $x_p = \pi d_p / \lambda$  the primary particle size parameter at wavelength  $\lambda$ ,  $\mathbf{T}_{jk}$  a  $3 \times 3$  matrix in terms of spherical Bessel functions,  $\mathbf{E}_{inc}$  the incident field, and  $s_j$  the coefficient for self-interaction. The above equation implies that the internal field of each particle in the aggregate is the sum of the phase difference induced by the incident radiation, multiple scattering induced by other particles in the aggregate, and self-interaction induced by the particle itself. The resulting extinction and absorption cross sections for aggregates with uniform particle sizes are found as follows, respectively:

$$C_{ext} = \frac{4\pi}{3k^2} \text{Im} \left[ (m^2 - 1) \sum_{j=1}^N x_{p_j}^3 \mathbf{E}_{inc}^* \cdot \mathbf{E}_j \right], \quad (2)$$

$$C_{abs} = \frac{4\pi}{3k^2} \text{Im}(m^2 - 1) \sum_{j=1}^N x_{p_j}^3 |\mathbf{E}_j|^2, \quad (3)$$

where complex conjugate is represented by asterisk and imaginary part of a complex quantity by Im. Total scattering cross section is obtained by subtracting absorption from extinction cross section.

An issue to be established before employing ICP computations are the number of orientations of individual aggregates and number of aggregates to be averaged to obtain statistically significant predictions. Farias et al<sup>17</sup> analyzed the required number of realizations in terms of number of primary particles in an aggregate, complex refractive index, scattering angle and particle diameter to obtain specific numerical accuracies for ICP predictions. Based on this study, 64 different aggregates of same size ( $N$ ), each sampled at 16 different orientations were averaged over in the present computations to have numerical uncertainties (95% confidence) less than 10%. These numbers were mainly determined by the differential scattering cross sections at large angles, where aggregate arrangements play a dominant role. Fewer realizations were needed for total scattering and absorption cross sections.

### Simulation of fractal aggregates

Large populations of aggregates had to be generated to study radiative characteristics of fractal geometries using the ICP method. Therefore, numerical simulations were performed to create aggregates that exhibit mass fractal properties, implying the following relationship between the number of particles in an aggregate,  $N$ , and the radius of gyration of the aggregate,  $R_g$ :<sup>4</sup>

$$N = k_f \left( \frac{R_g}{d_p} \right)^{D_f}, \quad (4)$$

where  $D_f$  and  $k_f$  are the fractal dimension and a prefactor, respectively. Recent measurements for a variety of soot aggregates in flame environments indicated that  $D_f = 1.7$ – $1.8$  and  $k_f = 8.5$ .<sup>3,7,8,24</sup>

Mass fractal-like aggregates were created using a practical procedure, which was previously employed by Farias et al<sup>17,25</sup> and Köylü et al,<sup>24</sup> in order to obtain particle positions in aggregates. The procedure involves a sequential algorithm which mimics Eq. (4), rather than performing numerical simulations based on the Langevin dynamics of Mountain and Mulholland.<sup>13</sup> With the

above specified values of  $D_f$  and  $k_f$ , the aggregate generation process was initiated by attaching individual and pairs of particles to each other randomly. The radius of gyration of the new aggregate was calculated by definition from the positions of each primary particles, and checked if it satisfied Eq. (4) with a fractal dimension of about 1.8. This procedure was continued in order to form progressively larger aggregates, obeying statistical relationships of mass fractal objects. It was observed that the fractal dimensions fell naturally in the range 1.6–1.9 for medium and large size aggregates, i.e., only few aggregates were rejected during these simulations.

For the purpose of investigating optical cross sections of polydisperse populations of aggregates, 64 different size aggregates were randomly selected such that the distribution of  $N$  had properties similar to a specified log-normal probability density function, which is represented by geometric mean,  $N_g$ , and geometric standard deviation,  $\sigma_N$ . However, particle diameters within each aggregate were kept constant. On the other hand, when polydisperse particle sizes were considered within each aggregates, the number of particles in aggregates were kept constant. The particle diameters were randomly created, following a specified Gaussian distribution, which is represented by arithmetic mean,  $\bar{d}_p$ , and standard deviation,  $\sigma_{d_p}$ . These two different distributions for  $N$  and  $d_p$  correspond to the transmission electron microscope (TEM) measurements of soot aggregates sampled from different flame environments.<sup>7,8</sup> Notice that monodisperse aggregates are represented by  $N = N_g$  and  $\sigma_N = 1$ , so that the mean aggregate sizes of polydisperse and monodisperse populations of aggregates are not equal because of the skewness of log-normal pdf's. But, this is not the case for particles since they are characterized by symmetric Gaussian pdf's, i.e., mean particle diameters of polydisperse and monodisperse populations of particles are equal, because the monodisperse case is given by  $d_p = \bar{d}_p$  and  $\sigma_{d_p} = 0$ .

Although it was desired to consider a broad range of aggregate sizes, there were computational limitations for the maximum  $N$  that can be studied using the ICP solution. Therefore, the specific ranges of aggregate and particle parameters used in this investigation were:  $N_g = 16$ –256,  $\sigma_N = 1, 2$  (corresponding to  $N = 2$ –808),  $\bar{x}_p = 0.1$ –0.3,  $\sigma_{d_p}/\bar{d}_p = 0, 0.15, 0.25$ ,  $D_f = 1.7$ –1.9, and  $k_f \cong 8.0$ . Projected images of typical aggregates constructed using the present simulations are shown in Fig. 1 for  $N = 16, 64, 256$  with monodisperse [Fig. 1(a)] and polydisperse [Fig. 1(b)] particle sizes. As discussed earlier, the simulated aggregates were mass-fractal like, satisfying Eq. (4). This behavior is illustrated in Fig. 2, which includes aggregate populations of  $N_g = 16, 64, 256$  with  $\sigma_N = 1, 2$ . The least-square fit to these simulations yielded  $D_f = 1.83$  and  $k_f = 7.9$  for  $N > 8$ . The figure also indicates that small aggregates deviate somewhat from the fractal behavior of the rest, since Eq. (4) starts failing as  $N \rightarrow 1$ .

#### RDG-FA approximate formulation

**Single aggregate.** The main results of Rayleigh–Debye–Gans theory for an aggregate with uniform size particles will be summarized in the following, since the complete formulation as well as relevant references can be found in Köylü and Faeth.<sup>3,8</sup>

Assuming that the particles that form aggregates satisfy the Rayleigh limit of Mie theory, and that the multiple scattering is negligible, RDG-FA approximation yields the differential scattering (for vertically or horizontally polarized incident and scattered light), total scattering and absorption cross sections as follows, respectively:

$$C_{vv}(\theta) = \left( \frac{C_{hh}}{\cos^2 \theta} \right) = N^2 C_{vv}^p f(qR_g) \quad (5)$$

$$C_{sca} = N^2 C_{sca}^p g(kR_g) \quad (6)$$

$$C_{abs} = N C_{abs}^p, \quad (7)$$

where  $\theta$  is the scattering angle,  $k = 2\pi/\lambda$ , and  $q = 2k \sin(\theta/2)$ . The superscript  $p$  denotes particle properties as given by Rayleigh theory (see, for example, Bohren and Huffman<sup>26</sup>),  $g(kR_g)$  is the aggregate total scattering factor. The form factor is obtained as:

$$f(qR_g) = \begin{cases} \exp \left[ -\frac{(qR_g)^2}{3} \right], & \text{Guinier regime,} \\ [(qR_g)^2]^{-D_f/2}, & \text{power-law regime,} \end{cases} \quad (8)$$

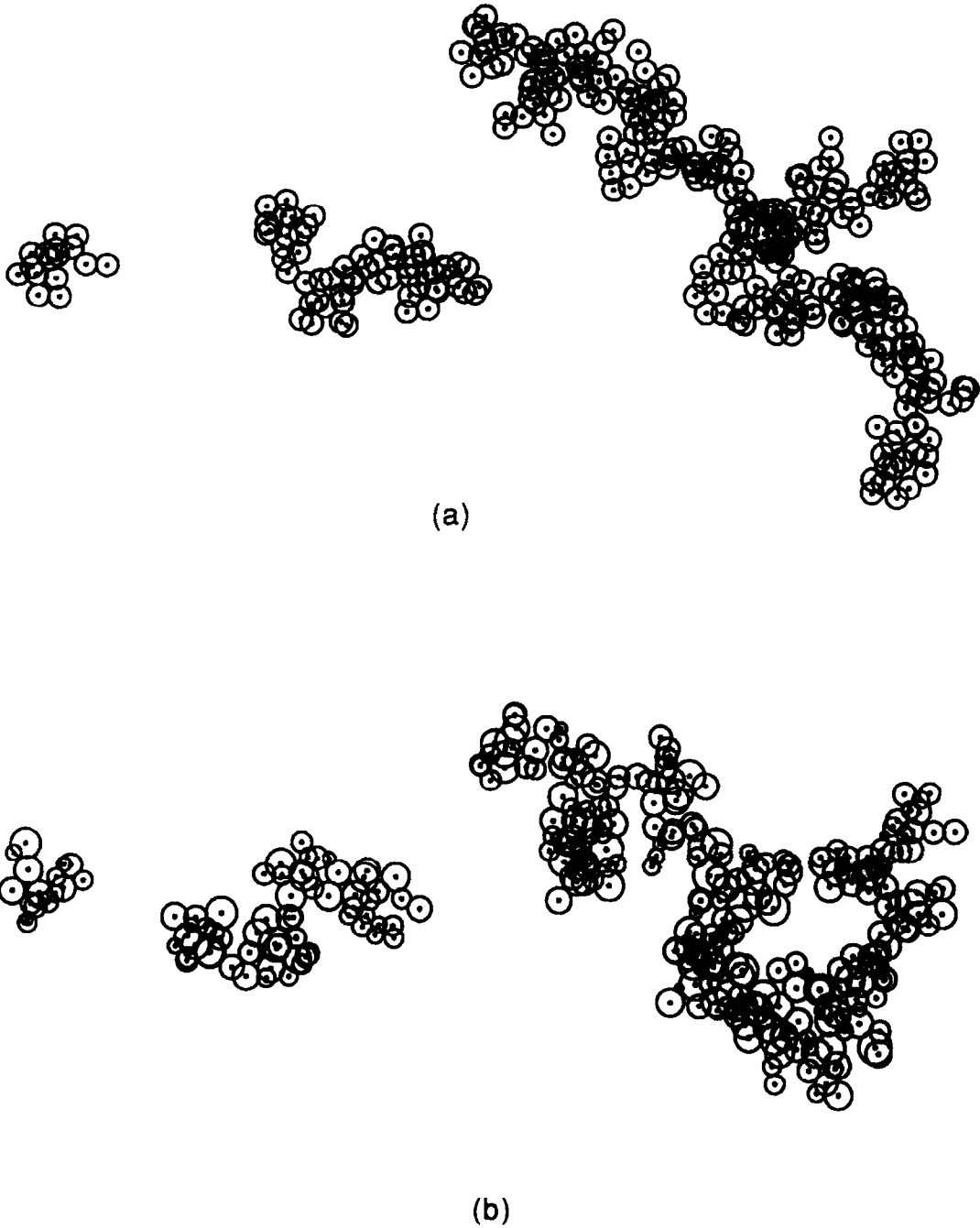


Fig. 1. Projected images of numerically simulated soot aggregates used in the ICP computations for  $N = 16, 64,$  and  $256$ : (a) monodisperse particles, (b) polydisperse particles ( $\sigma_w/d_p = 0.25$ ).

where the crossover between the Guinier and power-law regimes is  $(qR_g)^2 = 3D_f/2$ , following Dobbins and Megaridis.<sup>5</sup> The RDG-FA theory is completed using Eq. (4), which relates  $N$  to  $R_g$ .

Since the RDG theory is a first-order approximation with negligible scattering, it is, in fact, a special case of the ICP method without the second and third terms in Eq. (1). This means that computations could be carried out using particle locations of simulated aggregates, similar to Mountain and Mulholland.<sup>13</sup> However, Dobbins and Megaridis<sup>5</sup> compared Eqs. (5)–(8) to the RDG computations of Mountain and Mulholland,<sup>13</sup> finding good agreement except possibly the angular scattering results in the power-law regime (which will be discussed later on). Thus, the

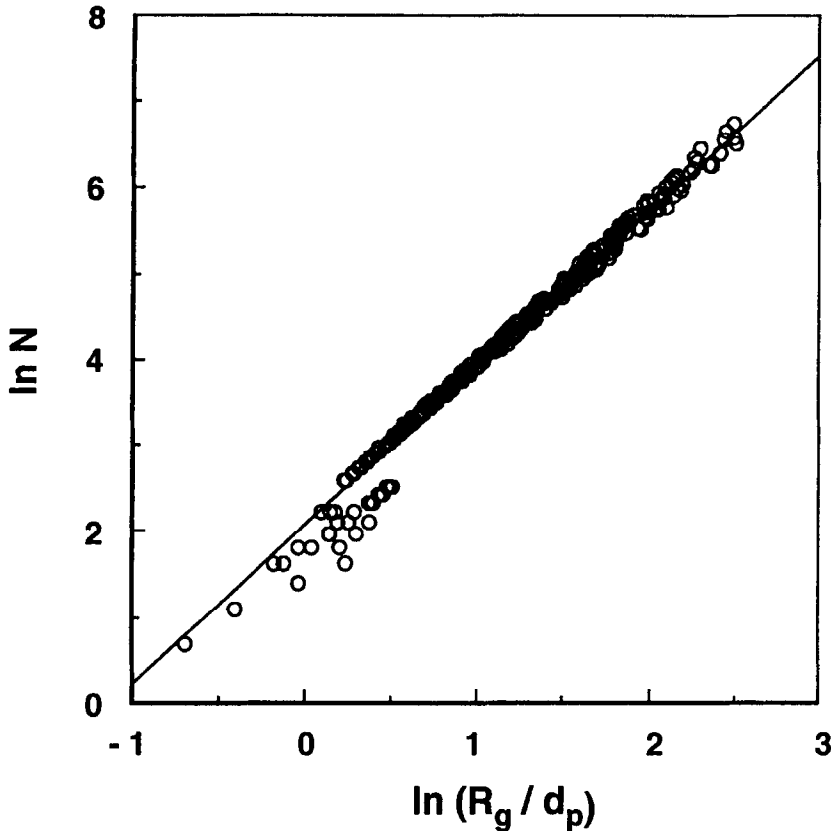


Fig. 2. Number of particles in aggregates as a function of radius of gyration normalized by particle diameter, yielding fractal dimension for simulated soot.

present study employs the above RDG-FA formulation of Eqs. (5)–(8) rather than RDG computations since, the optical cross sections of mass fractal aggregates similar to soot can be easily calculated using RDG-FA approximation, if the morphology of aggregates ( $d_p$ ,  $N$ ,  $D_f$ ,  $k_f$ ) is known, or vice versa. Moreover, these optical cross sections can be easily related to soot radiative characteristics such as albedo, phase function, extinction coefficient and emissivity. Accordingly, reasonable radiation heat transfer predictions from soot containing flames can be accomplished using RDG-FA theory, without heavy computations.

The RDG-FA formulation demonstrates that the optical properties of aggregates are substantially different from those of particles composing them. For example, Eqs. (5) and (6) imply that the aggregation enhances angular scattering by  $Nf(qR_g)$  and total scattering by  $Ng(kR_g)$  over the sum of the individual contributions of particles in the aggregate. On the contrary, Eq. (7) indicates that absorption is not affected by aggregation. Additionally, Eq. (8) testifies that the radius of gyration is the only determining property in the Guinier (small-angle) regime, while fractal dimension appears solely in the power-law regime. This means that angular scattering patterns are sensitive to the structure of the scatterer entirely in the power-law regime.

*Polydisperse aggregates.* The mean optical cross sections of populations of randomly oriented polydisperse aggregates are found by integrating over all aggregate sizes, as follows:

$$C_j(\sigma_N) = \int_{N=1}^{\infty} C_j(N)p(N) dN; \quad j = \text{vv(hh), sca, abs}, \quad (9)$$

where monodisperse aggregate cross sections (with  $N = N_g$ ,  $\sigma_N = 1$ ) are given by Eqs. (5)–(8), and  $p(N)$  is the log-normal aggregate size distribution function. It should be mentioned that this formal integration over the entire distribution is essential, since no single parameter, alone, can represent the scattering properties of polydisperse aggregates. Although numerical integration is generally

involved in evaluating Eq. (9), simple expressions for the mean cross sections from polydisperse aggregates,  $C_j(\sigma_N)$ , can still be obtained in terms of monodisperse properties,  $C_j$ , for special cases of angular and total scattering, and for all cases of absorption as follows:

$$\frac{C_j(\sigma_N)}{C_j} = \exp[\beta(\ln \sigma_N)^2]; \quad j = \text{vv(hh), sca, abs}, \quad (10)$$

where  $\beta = 1/2$  and 2 represent the angular and total scattering properties in the special case of all the aggregates being in the power-law regime [i.e.,  $p(N) \ll 1$  for small aggregates] and Guinier regime [i.e.,  $p(N) \ll 1$  for large aggregates], respectively. On the other hand, Eq. (10) with  $\beta = 1/2$  is valid for the mean absorption cross sections for any log-normally distributed aggregate sizes. Notice that the right-hand side of Eq. (10) also is directly related to the first and second moments of a log-normal distribution function.

*Polydisperse particles.* Within the RDG-FA approximation, the scattered field far from an aggregate is determined by a vector summation of the phase differences from various individual particles. In other words, the interference from each particle in the far-field is characterized by the relative position of the particle with respect to others and its volume. Since averaging over all possible orientations of an aggregate is accounted for in the development of RDG-FA, the sum of phase shifts from polydisperse particles with a symmetric size distribution (e.g., Gaussian) should be approximately equal to the case of monodisperse particles with the same mean diameter. Thus, the main assumption of the proposed modification of the RDG-FA approximation due to particle polydispersity is that the relative particle positions contribution to the scattered field is not affected by polydispersity, as long as the volume change of particles due to distribution is accounted for. Then, the following mean expressions for a Gaussian distribution of particles in aggregates can be obtained for differential and total scattering, and absorption cross sections, respectively:

$$\frac{C_j(\sigma_{d_p})}{C_j} = [V(\sigma_{d_p}/\bar{d}_p)]^2; \quad j = \text{vv(hh), sca}, \quad (11)$$

$$\frac{C_{\text{abs}}(\sigma_{d_p})}{C_{\text{abs}}} = V(\sigma_{d_p}/d_p), \quad (12)$$

where monodisperse particle cross sections (with  $d_p = \bar{d}_p$ ,  $\sigma_{d_p} = 0$ ) are given by Eqs. (5)–(8). The correction factor,  $V(\sigma_{d_p}/\bar{d}_p)$ , the ratio of the third moments of the polydisperse and monodisperse distributions, is found as:

$$V(\sigma_{d_p}/\bar{d}_p) = 1 + 3\left(\frac{\sigma_{d_p}}{\bar{d}_p}\right)^2. \quad (13)$$

Equation (11) serves as an approximation to estimate scattering, while Eq. (12) exactly holds for absorption.

## RESULTS AND DISCUSSION

### *Comparison of radiative models*

The phase function is illustrated in Fig. 3 as a function of scattering angle for monodisperse aggregates containing  $N = 128$  monodisperse particles with an optical size parameter of  $x_p = 0.3$ , which corresponds to the typical soot diameters at visible wavelengths. ICP results and the following approximate radiative models are shown: Mie theory for volume-equivalent sphere, Rayleigh limit for individual particles, RDG-FA formulation using Eq. (4) to relate  $N$ ,  $R_g$  and  $D_f$ , and RDG computational results obtained by applying Eq. (1) without the second and third terms and directly using particle positions in the simulated aggregates. Predictions of both Mie and Rayleigh theory do not follow the ICP results in magnitude and trend, clearly demonstrating the deficiency of spherical radiative models to represent aggregated soot particles. Although the RDG-FA formulation is in excellent agreement with ICP solution in the Guinier (small-angle) regime, the comparison becomes less satisfactory in the power-law (large-angle) regime. The same tendency was reported by Farias et al.,<sup>17</sup> in which the differences were attributed to the problems in ICP computations due to truncation errors. This seemed to be reasonable since ICP predictions

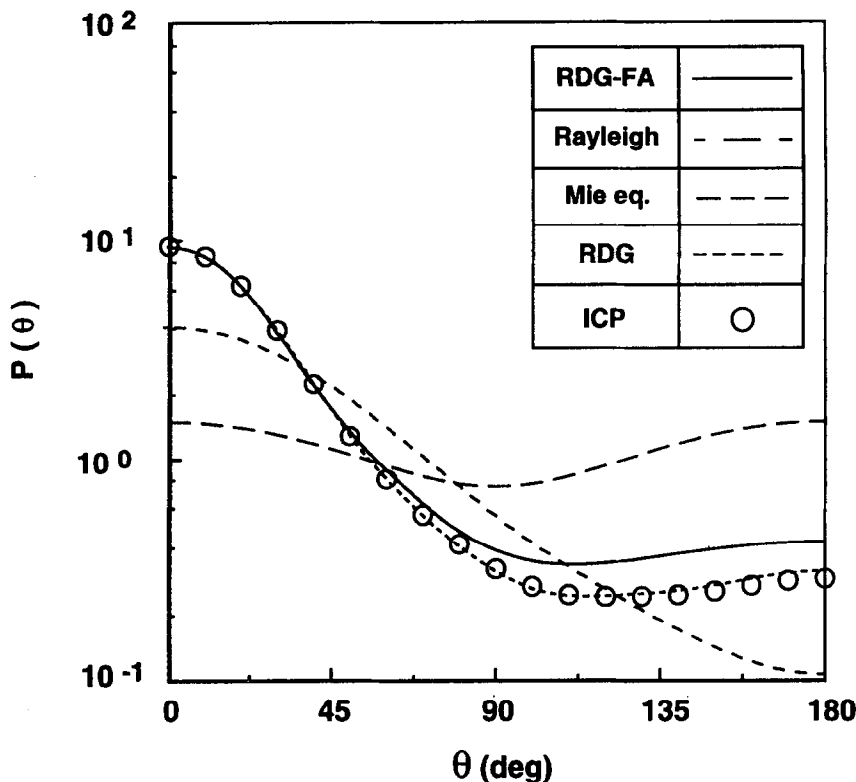


Fig. 3. Various predictions of phase function as a function of scattering angle for an aggregate with  $N = 128$ ,  $x_p = 0.3$ .

rather than RDG-FA formulation contradicted experimental observations in the power-law regime, in which the slope of  $C_{vv}$  vs  $q$  curves yielded  $-D_f$ , as depicted by Eq. (8). However, Fig. 3 indicates that the ICP results are identical to the RDG computational predictions, which employed the particle positions directly instead of Eq. (4). Thus, an artifact of the simulated aggregates appears to be responsible for the differences between ICP/RDG computational results and RDG-FA formulation in the power-law regime. Similar behavior (although not discussed explicitly) can be observed in the results of other computational studies, which employed aggregate simulations.<sup>5,13,15</sup> Noting that the angular scattering pattern in the power-law regime is extremely sensitive to the morphology and orientation of the computer-generated aggregates, this attests that there may be some minor differences between individually created aggregates and the statistical relationship of Eq. (4). Fortunately, the results of the present study are affected insignificantly by this behavior in the power-law regime. Nevertheless, the detail characterization of fractal aggregates using computer simulations evidently merits additional investigation.

The above discussion suggests that the RDG-FA predictions of phase function, in fact, are in excellent agreement with ICP results, aside from the power-law regime due to uncertainties regarding the fractal properties of computer-generated soot aggregates. This encouraging performance of RDG-FA approximation also is supported by Table 1, which summarizes the normalized cross sections of forward scattering, total scattering and absorption. The results of ICP computations and RDG-FA formulation of Eqs. (5)–(8) are tabulated for aggregates with  $N = 16$ –256 and  $x_p = 0.1$ –0.3. Although there were isolated differences of up to 15% in total scattering cross section, the RDG-FA and ICP predictions generally agreed within 10% for the present conditions. This implies that the multiple scattering should be negligible for soot aggregates, verifying that  $C_{vv}(0^\circ) \approx N^2 C_{vv}^p$  and  $C_{abs} \approx N C_{abs}^p$ . Hence, the RDG-FA theory appears to be the most reliable approximate model to treat the radiative properties of aggregated soot particles. Finally, it should be noted that the cross sections in Table 1 are for monodisperse particles and aggregates, which will be used as baseline values in comparison to polydisperse cases, later on.

Table 1. ICP and RDG-FA predictions of soot optical cross sections.

N	x <sub>p</sub>	k <sup>2</sup> C <sub>w</sub> (θ = 0°)		k <sup>2</sup> C <sub>sca</sub>		k <sup>2</sup> C <sub>abs</sub>	
		ICP	RDG-FA	ICP	RDG-FA	ICP	RDG-FA
16	0.1	5.87 × 10 <sup>-5</sup>	5.67 × 10 <sup>-5</sup>	4.61 × 10 <sup>-4</sup>	4.47 × 10 <sup>-4</sup>	5.50 × 10 <sup>-2</sup>	5.31 × 10 <sup>-2</sup>
	0.3	4.41 × 10 <sup>-2</sup>	4.13 × 10 <sup>-2</sup>	2.20 × 10 <sup>-1</sup>	1.91 × 10 <sup>-1</sup>	1.57	1.43
32	0.1	2.32 × 10 <sup>-4</sup>	2.27 × 10 <sup>-4</sup>	1.75 × 10 <sup>-3</sup>	1.65 × 10 <sup>-3</sup>	1.13 × 10 <sup>-1</sup>	1.06 × 10 <sup>-1</sup>
	0.3	1.73 × 10 <sup>-1</sup>	1.65 × 10 <sup>-1</sup>	5.83 × 10 <sup>-1</sup>	5.52 × 10 <sup>-1</sup>	3.01	2.87
64	0.1	9.47 × 10 <sup>-4</sup>	9.07 × 10 <sup>-4</sup>	6.01 × 10 <sup>-3</sup>	5.42 × 10 <sup>-3</sup>	2.26 × 10 <sup>-1</sup>	2.12 × 10 <sup>-1</sup>
	0.3	6.64 × 10 <sup>-1</sup>	6.61 × 10 <sup>-1</sup>	1.43	1.44	5.91	5.73
96	0.1	2.13 × 10 <sup>-3</sup>	2.04 × 10 <sup>-3</sup>	1.16 × 10 <sup>-2</sup>	9.61 × 10 <sup>-3</sup>	3.39 × 10 <sup>-1</sup>	3.18 × 10 <sup>-1</sup>
	0.3	1.46	1.49	2.39	2.45	8.80	8.60
128	0.1	3.77 × 10 <sup>-3</sup>	3.63 × 10 <sup>-3</sup>	1.74 × 10 <sup>-2</sup>	1.59 × 10 <sup>-2</sup>	4.51 × 10 <sup>-1</sup>	4.25 × 10 <sup>-1</sup>
	0.3	2.56	2.64	3.18	3.55	11.59	11.46
256	0.1	1.50 × 10 <sup>-2</sup>	1.45 × 10 <sup>-2</sup>	5.06 × 10 <sup>-2</sup>	4.42 × 10 <sup>-2</sup>	9.00 × 10 <sup>-1</sup>	8.49 × 10 <sup>-1</sup>
	0.3	9.83	10.57	7.31	8.41	22.51	22.93

Effects of aggregate polydispersity

Since aggregates had to be generated using computer simulations to employ ICP method, polydisperse populations of aggregates were studied using 64 aggregates with different N, satisfying a specified log-normal pdf for each distribution. As a result, RDG-FA predictions were obtained using the parameters of the same 64 aggregates so that a meaningful comparison to ICP results is possible. Accordingly, summations over the discrete populations were involved for calculating mean cross sections, instead of formal integrations over the continuous distributions using Eq. (9). The RDG-FA calculations for the mean properties using the discrete pdf's did not differ from the continuous ones more than 10%, except for the largest aggregates with N<sub>g</sub> = 256, σ<sub>N</sub> = 2, which had to be truncated for N > 808 due to computational time and storage limitations in ICP

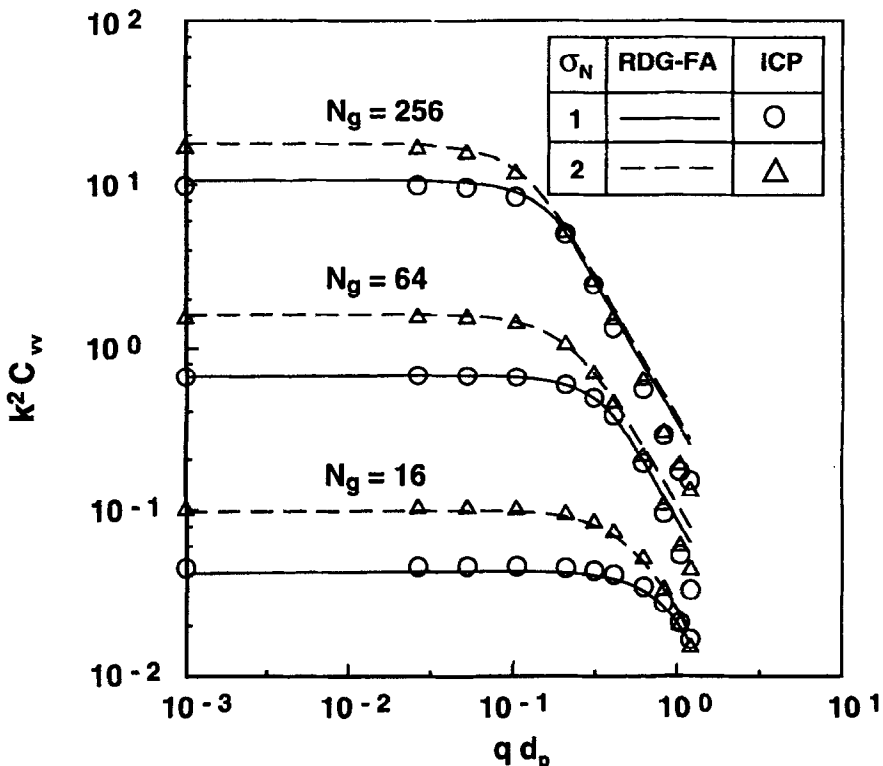


Fig. 4. Normalized differential scattering cross section as a function of normalized modulus of the scattering vector for monodisperse (N = 16, 64, 256 and σ<sub>N</sub> = 1) and polydisperse (N<sub>g</sub> = 16, 64, 256 and σ<sub>N</sub> = 2) aggregate populations.

calculations. The same computational considerations restricted the present investigation to a maximum geometric standard deviation of 2.

Figure 4 is an illustration of ICP and RDG-FA predictions for the normalized mean angular scattering cross section,  $k^2 C_{vv}$ , as a function of the normalized modulus of the scattering vector,  $qd_p$ , for polydisperse ( $\sigma_N = 2$ ) and monodisperse ( $\sigma_N = 1$ ) aggregate populations with  $D_f = 1.8$ ,  $k_f = 8.0$ . The uniform size particles in aggregates have  $x_p = 0.3$  and  $m = 1.57 + 0.57i$ , representative of soot at visible wavelengths.<sup>3</sup> The monodisperse results in Fig. 4 indicate that the scattered amount of light increases as the aggregates become bigger. Furthermore, the Guinier (small-angle) regime shrinks while power-law (large-angle) regime expands, yielding larger dissymmetry ratios, as  $N$  changes from 16 to 256. RDG-FA predictions are in excellent agreement with ICP results, except at large scattering angles. As discussed previously, these minor differences in the power-law regime should not be interpreted as a handicap of RDG-FA method, but rather as an artifact of computer-simulated aggregates used in ICP computations, since the slope of RDG-FA predictions at large angles accurately yields a fractal dimension of 1.8, consistent with earlier experimental observations.<sup>3,8,14</sup>

As can be seen from Fig. 4, the effect of polydispersity of aggregates on the angular scattering is obvious in the Guinier regime, i.e., the mean angular scattering is enhanced over the monodisperse case. However, the mean scattering cross sections from polydisperse aggregates do not seem to be different from the monodisperse case in the power-law regime. In fact, if the first moments of the monodisperse and polydisperse populations were the same, the results of both cases would be exactly the same. These two different behaviors in the angular scattering pattern can be explained by noting that  $C_{vv}(\sigma_N)$  in the power-law and Guinier regimes is proportional to the first ( $\bar{N}$ ) and second ( $\overline{N^2}$ ) moments of the aggregate size distribution function, respectively. In consistent with this observation, Fig. 4 shows  $N_g = 256$  case being less modified than  $N_g = 16$  case by polydispersity. In other words, there will be no difference between polydisperse and monodisperse cases in the limit of large aggregates, since the scattering pattern will be completely dominated by power-law regime. Finally, the RDG-FA approximation accurately predicts the mean cross sections from polydisperse populations of aggregates, yielding good agreement with ICP results for the conditions considered in Fig. 4. It should be mentioned that the angular scattering results of  $x_p = 0.1$  case as well as other aggregate populations were similar, and, therefore, will not be discussed.

The ratios of mean optical cross sections from polydisperse ( $\sigma_N = 2$ ) to monodisperse ( $\sigma_N = 1$ ) populations of aggregates are presented as a function of geometric mean aggregate size,  $N_g$ , of the distributions in Fig. 5. The predictions of ICP and RDG-FA for forward scattering ( $\theta = 0^\circ$ ), total scattering and absorption cross sections are included for  $x_p = 0.1$  and 0.3. The ICP results shown in Fig. 5 point out that the aggregate polydispersity with  $\sigma_N = 2$  enhances the forward scattering and absorption by a factor of 2.4 and 1.25, respectively over the monodisperse cases. Additionally, the effects of polydispersity in  $N$  (or  $R_g$ ) on forward scattering and absorption cross sections appear to be independent of  $N_g$ . On the other hand, Fig. 5 illustrates that the influence of polydispersity on the behavior of the total scattering cross section is somewhat complex, i.e., the ratios of the mean properties of polydisperse aggregates to monodisperse cases decrease with increasing  $N_g$  and  $x_p$ .

The RDG-FA predictions in Fig. 5 generally agree with ICP results within 10%, using the discrete populations with each having 64 aggregate sizes. However, continuous distribution functions should be considered in real flames conditions. Then, Eq. (10) with  $\sigma_N = 2$  will yield a ratio of 2.61 for forward scattering and total scattering in the limit of small  $N_g$  ( $\beta = 2$ ), and 1.27 for absorption and total scattering in the limit of large  $N_g$  ( $\beta = 0.5$ ). Thus, the forward scattering from polydisperse aggregates is approximately proportional to  $\overline{N^2}$ , while backward scattering and absorption are directly related to  $\bar{N}$ , as correctly predicted by the RDG-FA formulation of the present study. This explicitly implies that the mean scattering properties from polydisperse aggregate populations can not be characterized by a single moment of the distribution, for example,  $R_g^2$ , as suggested by Dobbins and Megaridis.<sup>5</sup>

#### *Effects of particle polydispersity*

This part of the study investigates mean optical cross sections from monodisperse aggregates with

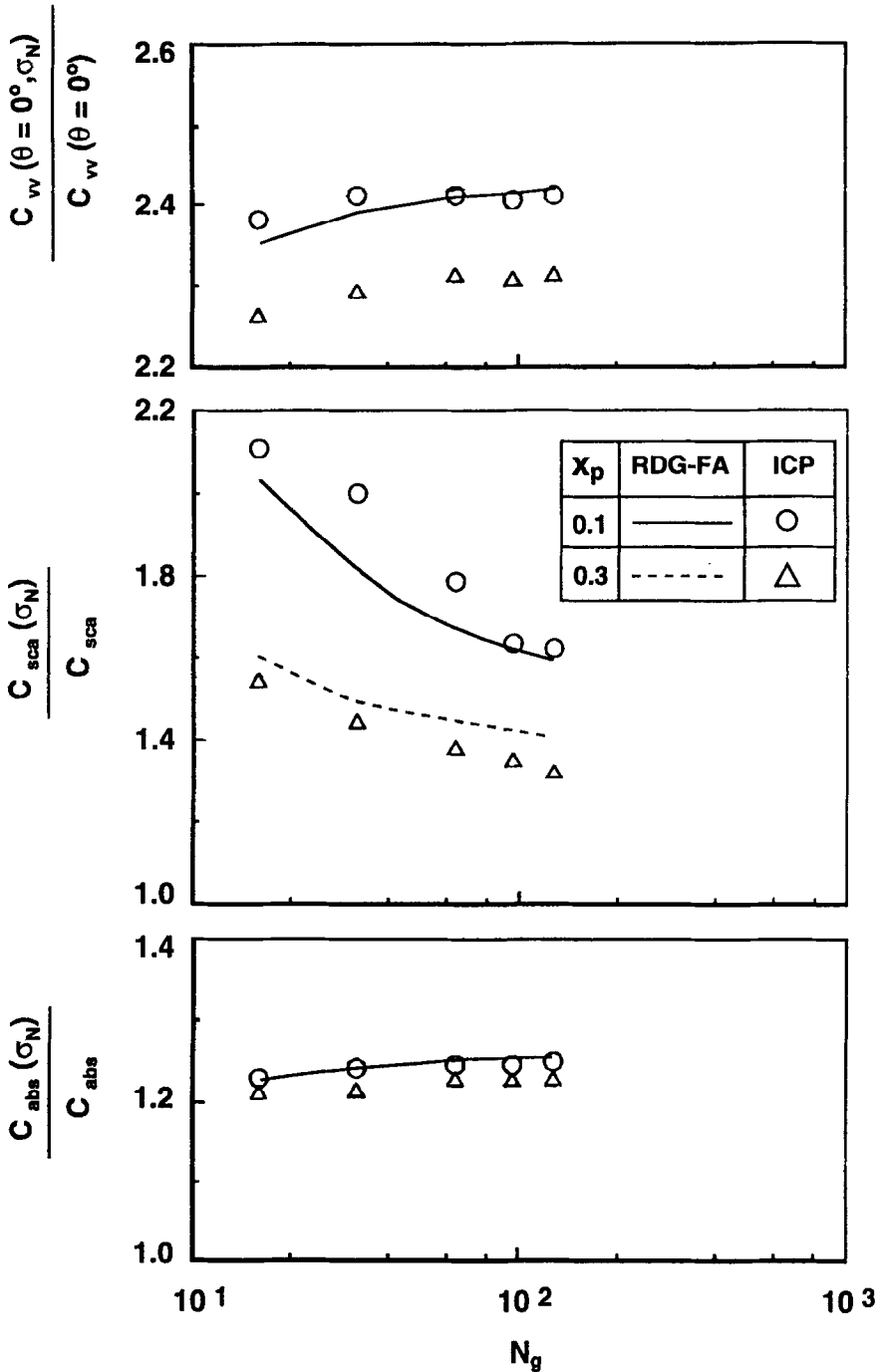


Fig. 5. The ratio of various mean optical cross sections from polydisperse ( $\sigma_N = 2$ ) to monodisperse ( $\sigma_N = 1$ ) aggregate cases as a function of  $N_g$  for  $x_p = 0.1$  and  $0.3$ .

polydisperse particle diameters. The particle size polydispersities are represented by Gaussian probability density functions, following TEM measurements of Köylü and Faeth.<sup>7,8</sup> Correspondingly, two different standard deviations of 15 and 25% of the mean diameter are chosen.

Figure 6 illustrates ICP and RDG-FA predictions of  $k^2 C_w$  as a function of  $qd_p$  for aggregates with  $D_f = 1.8$  and  $k_f = 8.0$ , formed by polydisperse ( $\sigma_{d_p}/\bar{d}_p = 0.25$ ) and monodisperse ( $\sigma_{d_p} = 0$ ) particles with  $\bar{x}_p = 0.3$  and  $m = 1.57 + 0.57i$ . Note that the results of monodisperse particles cases in Fig. 6 are identical to the corresponding results of monodisperse aggregates cases

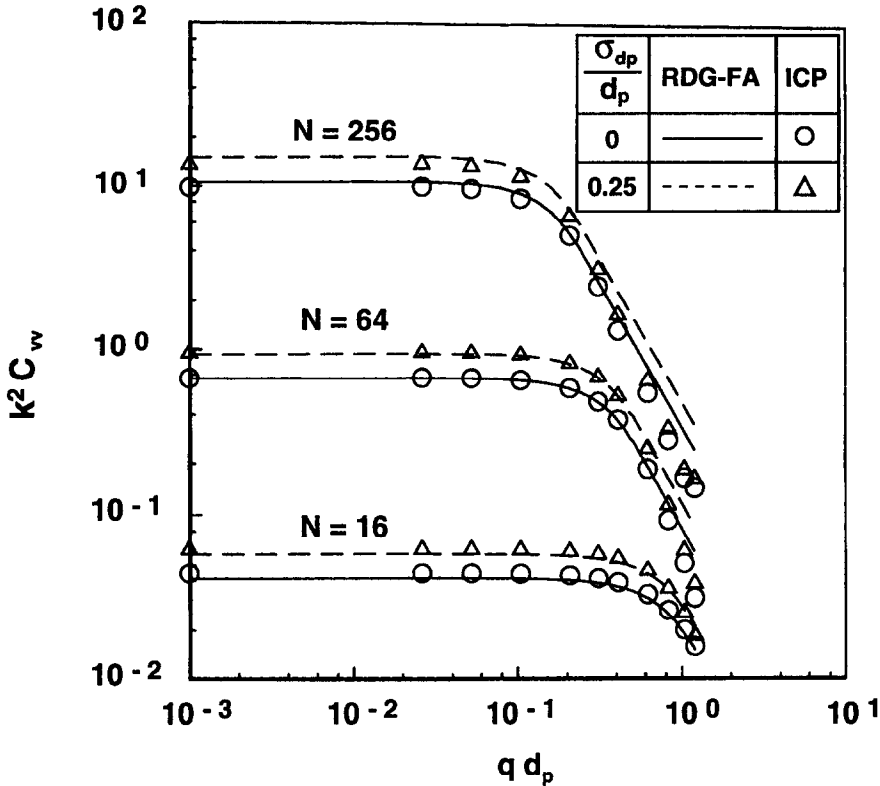


Fig. 6. Normalized differential scattering cross section as a function of normalized modulus of the scattering vector for aggregates containing monodisperse ( $N = 16, 64, 256$  and  $\sigma_{dp} = 0$ ) and polydisperse ( $N = 16, 64, 256$  and  $\sigma_{dp}/\bar{d}_p = 0.25$ ) particles with  $\bar{x}_p = 0.3$ .

in Fig. 4. However, the first thing to notice from the ICP predictions in Fig. 6 is that the influence of particle polydispersity on the angular scattering pattern is rather different from the influence of aggregate polydispersity shown in Fig. 4. First, the enhancement of the mean angular scattering cross sections due to particle size distribution function is small compared to aggregate size polydispersity, because of relatively narrow distribution of particle diameters. In addition, the influence of particle polydispersity is the same for all aggregate size and scattering angles. However, this effect seems to be less pronounced in the power-law regime, in which the ICP results for polydisperse particles are difficult to distinguish from the monodisperse particles case. Finally, the RDG-FA formulation, modified to account for polydisperse particle populations, appears to yield good agreement compared to ICP results.

The relative effects of polydispersity of particles in aggregates on various optical properties are plotted as a function of aggregate size in Fig. 7, which includes ICP and RDG-FA predictions for two mean diameters, corresponding to  $\bar{x}_p = 0.1$  and  $0.3$ , and two relative standard deviations of  $\sigma_{dp}/\bar{d}_p = 0.15$  and  $0.25$ . ICP computations of forward scattering, total scattering and absorption cross sections point out that the relative effect of particle polydispersity is nearly independent of  $N$  and  $\bar{x}_p$ , implying that the relative standard deviation of particle sizes is the only controlling parameter. ICP results in Fig. 7 also suggest that the forward and total scattering cross sections are increased by the same amount of 14 and 41% due to particle polydispersity considerations, as precisely predicted by RDG-FA modified formulation of Eq. (11). Meanwhile, Eq. (12) with  $\sigma_{dp}/\bar{d}_p = 0.15$  and  $0.25$  yield values of 1.07 and 1.19, respectively, which are identical to the ICP predictions of absorption in Fig. 7. Thus, RDG-FA approximate theory accurately predicts the mean optical cross sections of soot from polydisperse populations of not only aggregates but also particles.

A comparison of the results plotted in Fig. 7 and Fig. 5 indicates that the influence of particle polydispersity on angular and total scattering is small compared to the influence of aggregate

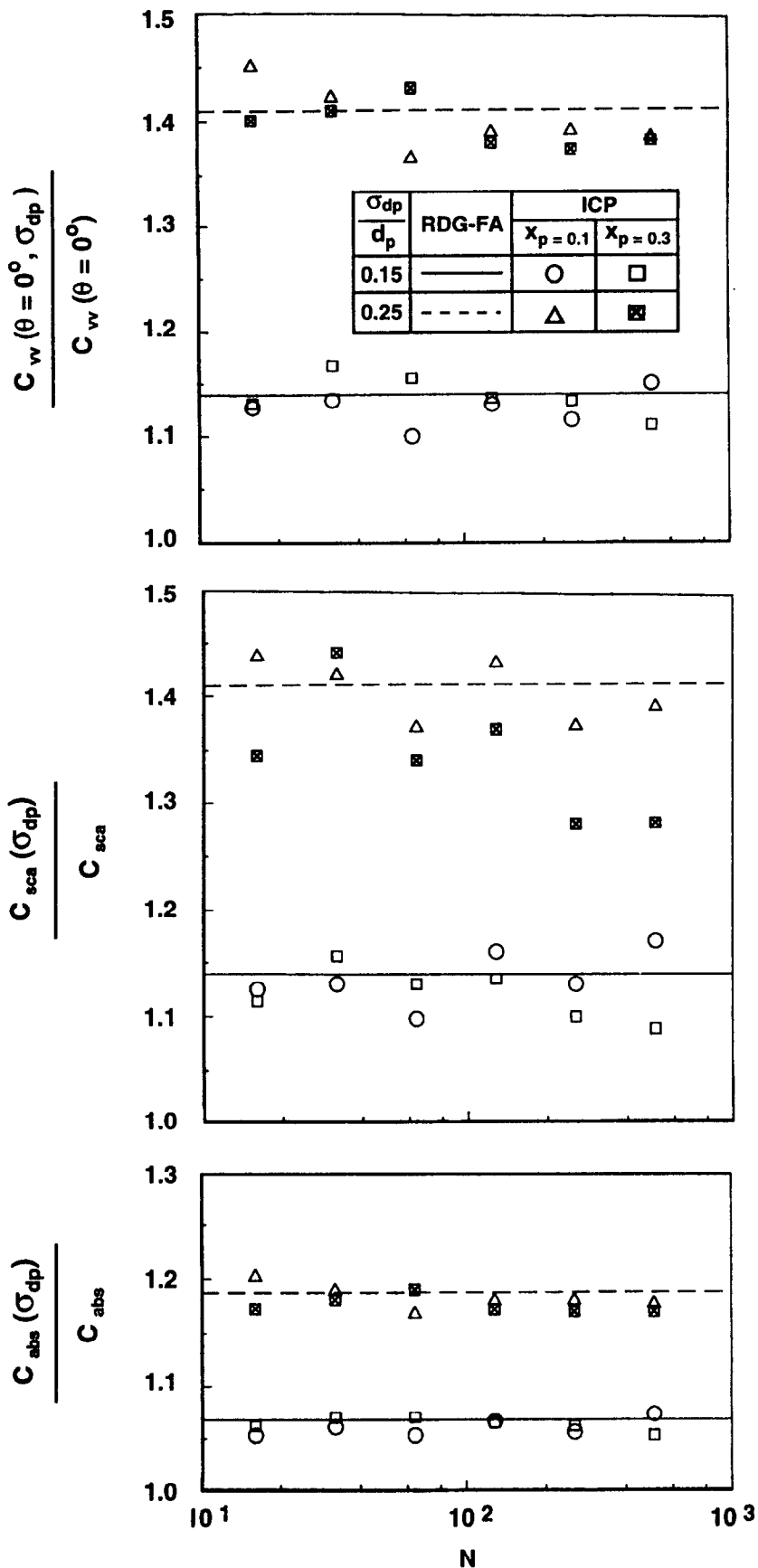


Fig. 7. The ratio of various mean optical cross sections from aggregates with polydisperse ( $\sigma_{dp}/\bar{d}_p = 0.15$  and  $0.25$ ) to monodisperse particle cases ( $\sigma_{dp} = 0$ ) as a function of  $N$  for  $X_p = 0.1$  and  $0.3$ .

polydispersity. However, this is not the case for the absorption cross section, which is enhanced by the polydispersity of particles and aggregates in a comparable manner. As a result, the distribution of particles in aggregates should be accounted for in RDG-FA estimates of absorption cross section, considering the importance of absorption mechanism in radiation heat transfer from soot containing flames.

## CONCLUSIONS

An evaluation of the effects of aggregate and particle size polydispersity on the optical properties of simulated soot was completed based on the ICP computations and RDG-FA formulation for mass fractal-like morphologies. Simple expressions were given to account for the polydispersity of particles and aggregates, which were represented by Gaussian and log-normal distribution functions, respectively. Specific ranges of aggregate and particle properties were selected to approximate soot found in flame environments:  $N_g = 16\text{--}256$ ,  $\sigma_N = 1$ , 2,  $\bar{x}_p = 0.1\text{--}0.3$ ,  $\sigma_{d_p}/\bar{d}_p = 0$ , 0.15, 0.25,  $D_f = 1.7\text{--}1.9$ ,  $k_f = 8.0$  and  $m = 1.57 + 0.57i$ , corresponding to the visible and near-infrared portions of the spectrum. The main conclusions of the study are summarized as follows:

1. ICP and RDG-FA predictions of soot optical cross sections for monodisperse aggregates and particles generally agreed within 10%, suggesting negligible multiple scattering for soot. However, there were minor differences between ICP and RDG-FA predictions of the differential scattering cross section in the power-law regime, which were shown to be an artifact of the computer-simulated aggregates used in ICP computations, rather than a handicap of the scattering methods.
2. The influence of polydispersity of aggregates on the mean differential scattering cross section was significant in the Guinier regime, while the power-law regime did not seem to be affected. Additionally, the mean forward scattering and absorption cross sections of polydisperse aggregates relative to the monodisperse cases were found to be independent of  $N_g$  and  $x_p$ , in contrast to the complex behavior of total scattering. The mean forward scattering cross section from polydisperse aggregates was approximately proportional to  $\bar{N}^2$ , whereas angular scattering in the power-law regime and absorption were governed by  $\bar{N}$ , emphasizing that no single parameter can characterize the optical properties of polydisperse aggregates.
3. The effect of particle polydispersity on the differential scattering cross section was similar for all aggregate sizes and scattering angles, but was less pronounced in the power-law regime. Results obtained for forward scattering, total scattering and absorption cross sections indicated that the relative effect of particle polydispersity on the mean optical properties solely depend upon the relative standard deviation of the particle size distribution.
4. Angular and total scattering properties were more enhanced by aggregate polydispersity than particle polydispersity. However, this was not the case for the absorption cross section, in which the effects of the polydispersity of particles and aggregates were comparable for the conditions of the study. Finally, the present RDG-FA approximate formulation accurately predicted the mean optical cross sections of polydisperse populations of soot aggregates as well as particles, identifying it as the most reliable approximate model to treat the radiative properties of aggregated soot particles.

*Acknowledgements*—T. L. Farias would like to acknowledge the scholarship from PRAXIS XXI (BD/2633/94). Ü. Ö. Köylü was partially supported by AFOSR (Grant No. 94-0143). The collaboration between Portugal and U.S.A. was sponsored by AGARD Support Project P-101. The authors are also indebted to G. M. Faeth for helpful discussions.

## REFERENCES

1. R. Siegel and J. R. Howell, *Thermal Radiation Heat Transfer*, Hemisphere, New York (1981).
2. Ü. Ö. Köylü and G. M. Faeth, *J. Heat Transfer* **115**, 409 (1993).
3. Ü. Ö. Köylü and G. M. Faeth, *J. Heat Transfer* **116**, 152 (1994).
4. R. Jullien and R. Botet, *Aggregation and Fractal Aggregates*, World Scientific, Singapore (1987).
5. R. A. Dobbins and C. M. Megaridis, *Appl. Opt.* **30**, 4747 (1991).
6. C. M. Megaridis and R. A. Dobbins, *Combust. Sci. Tech.* **71**, 95 (1990).
7. Ü. Ö. Köylü and G. M. Faeth, *Combust. Flame* **89**, 140 (1992).

8. Ü. Ö. Köylü and G. M. Faeth, *J. Heat Transfer* **116**, 971 (1994).
9. A. R. Jones, *Proc. Roy. Soc. London A* **366**, 111 (1979).
10. D. S. Saxon, *The UCLA International Conference on Radiation and Remote Probing of the Atmosphere* (Ed. J. G. Kuriyan), p. 227 (1974).
11. M. V. Berry and I. C. Percival, *Optica Acta* **33**, 577 (1987).
12. J. E. Martin and A. J. Hurd, *J. Appl. Cryst.* **20**, 61 (1987).
13. R. D. Mountain and G. W. Mulholland, *Langmuir* **4**, 1321 (1988).
14. C. M. Sorensen, J. Cai, and N. Lu, *Langmuir* **8**, 2064 (1992).
15. S. B. Singham and C. F. Bohren, *Langmuir* **9**, 1431 (1993).
16. G. W. Mulholland, C. F. Bohren, and K. A. Fuller, *Langmuir* **10**, 2533 (1994).
17. T. L. Farias, M. G. Carvalho, Ü. Ö. Köylü, and G. M. Faeth, *J. Heat Transfer* **117**, 152 (1995).
18. M. F. Iskander, H. Y. Chen, and J. E. Penner, *Appl. Opt.* **28**, 3083 (1989).
19. P. B. Sunderland, Ü. Ö. Köylü, and G. M. Faeth, *Combust. Flame* **100**, 310 (1995).
20. J. C. Ku and K.-H. Shim, *JQSRT* **47**, 201 (1992).
21. E. M. Purcell and C. R. Pennypacker, *Astrophys. J.* **186**, 705 (1973).
22. G. H. Goedecke and S. G. O'Brien, *Appl. Opt.* **27**, 2431 (1988).
23. T. L. Farias, Ph.D. Thesis, Instituto Superior Técnico, Lisbon, in preparation.
24. Ü. Ö. Köylü, G. M. Faeth, T. L. Farias, and M. G. Carvalho, *Combust. Flame* **100**, 621 (1995).
25. T. L. Farias, M. G. Carvalho, Ü. Ö. Köylü, and G. M. Faeth, *Int. J. Heat Tech.*, in press.
26. C. F. Bohren and D. R. Huffman, *Absorption and Scattering of Light by Small Particles*, Wiley, New York (1983).